Molecular dynamics simulations of hydrogen bombardment of tungsten carbide surfaces

P. Träskelin,[1] N. Juslin,[1] P. Erhart,[2] and K. Nordlund[1]
[1]*Association EURATOM-Tekes, Accelerator Laboratory, University of Helsinki, P.O. Box 43, FIN-00014, Finland*
[2]*Institut für Materialwissenschaft, Technische Universität Darmstadt, Petersenstraße 23, D-64287 Darmstadt, Germany*
(Received 21 April 2006; revised manuscript received 20 November 2006; published 23 May 2007)

The interaction between energetic hydrogen and tungsten carbide (WC) is of interest both due to the use of hydrogen-containing plasmas in thin-film manufacturing and due to the presence of WC in the divertor of fusion reactors. In order to study this interaction, we have carried out molecular dynamics simulations of the low-energy bombardment of deuterium impinging onto crystalline as well as amorphous WC surfaces. We find that prolonged bombardment leads to the formation of an amorphous WC surface layer, regardless of the initial structure of the WC sample. Loosely bound hydrocarbons, which can erode by swift chemical sputtering, are formed at the surface. Carbon-terminated surfaces show larger sputtering yields than tungsten-terminated surfaces. In both cumulative and noncumulative simulations, C is seen to sputter preferentially. Implications for mixed material erosion in ITER are discussed.

DOI: 10.1103/PhysRevB.75.174113 PACS number(s): 79.20.Ap, 82.20.Wt, 34.50.Dy, 52.40.Hf

I. INTRODUCTION

Tungsten carbide (WC) exhibits extraordinary hardness and temperature resistance. It has long been applied in the form of cemented carbide (using cobalt binder), which provides not only very hard and abrasion resistant but also very tough hard metals, used, for example, for cutting and mining tools, wear parts, and fine drills. The fabrication of WC thin films often involves the use of hydrogen-containing plasmas, making it important to understand its plasma-surface interactions.[1–3]

Understanding the interaction of hydrogen plasmas with WC is furthermore of particular interest for fusion reactor design. In some existing conceptual fusion reactors as well as the next-generation reactor ITER, the divertor armor is designed to consist predominantly of carbon fiber composites and tungsten (W) with carbon coatings in the areas subject to the highest heat load.[4,5] Carbon is advantageous because of its low atomic number and excellent thermophysical properties but is also known to efficiently trap hydrogen especially in codeposited layers.

The purpose of a divertor in a tokamaklike fusion reactor is to be the target for particle exhaust and redirect impurities into regions remote from the core plasma. During operation, the entire divertor will be subject to intense bombardment by low-energy (1–100 eV) hydrogen isotopes, giving rise to small hydrocarbon molecule erosion as well as hydrogen bubble formation.[6–8] The eroded hydrocarbons are known to drift in the reactor and form hydrocarbon films on other plasma facing parts of the chamber, including the tungsten parts.[9] Metal carbides are naturally present at the interfaces between the carbon first wall and the metallic parts underneath. Moreover, they can also be formed when hydrocarbon molecules, eroded under particle bombardment, react with metal parts in other sections of the plasma chamber. Because of the abundance of tungsten, the most relevant metal carbide to be considered in this context is WC.

Sputtering yields in WC have been measured by a few groups.[10–14] The results show that preferential sputtering of carbon plays a big role for the erosion of WC (Ref. 10) and that at least part of the sputtering is chemical in origin.[11] However, the binary collision approximation simulations used until now for analyzing the experimental results capture neither chemical sputtering nor the details of the surface structure of the samples.

In this work, we present molecular dynamics simulations on the bombardment of both crystalline and amorphous WC surfaces with energetic hydrogen from a plasma. In order to model the complex interactions in the W-C-H system, we employed a recently developed reactive bond-order potential which is capable of describing both the pure and the compound phases at a high level of precision.[15] For the present application, it is of particular importance that this potential has been shown to provide a good description of both C_xH_y and WH_x molecules, hydrogen in tungsten as well as the thermal and surface properties of tungsten carbide. Since under operation conditions crystalline as well as amorphous tungsten-carbon interfaces can form, we considered both crystalline and amorphous cells. The latter furthermore allow us to study systematically the effect of carbon incorporation and potential surface amorphization on the performance of tungsten parts. We further note that our simulations of crystalline tungsten carbide show surface amorphization at certain energies which provides further motivation for studying amorphous W_xC_{1-x} structures explicitly. We carried out cumulative as well as noncumulative bombardment simulations using deuterium ions, since this isotope has been the most widely employed in experiments in this field. However, the results for other hydrogen isotopes can be expected to be similar except for a mass scaling factor.[7] Based on our simulations, we are able to predict tungsten and carbon sputtering yields for surfaces of different morphology and composition as well as the evolution of the composition of the cell.

The remainder of this paper is organized as follows. The following section details the setup of the simulations and the generation of the simulation cells. The results for crystalline tungsten carbide are presented and discussed in Sec. III while Sec. IV summarizes the results obtained with amorphous cells. The results are discussed and compared to experiments in Sec. V.

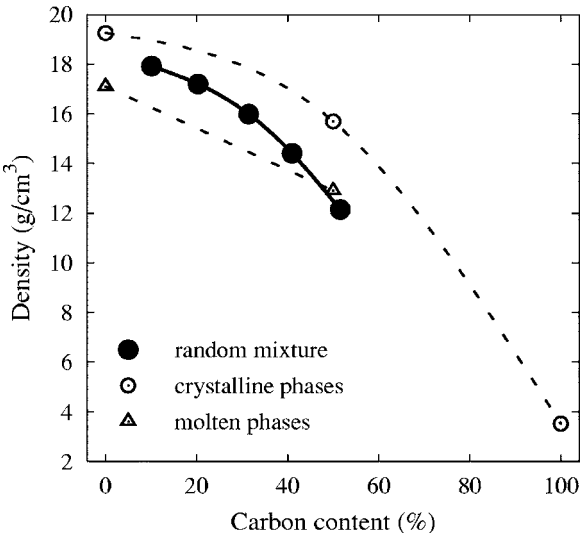

FIG. 1. Variation of density with carbon content in the as-created simulation cells.

II. METHOD

The ground-state structure of tungsten carbide has a hexagonal symmetry (space-group $P\bar{6}m2$, lattice index symbol B_h). It can be conveniently pictured as a hexagonal-close-packed lattice with an axial ratio of $c/a \approx 0.97$ whose A and B layers along the c axis are occupied by tungsten and carbon atoms, respectively.

Both crystalline and amorphous samples were studied. The crystalline cells comprised $8 \times 5 \times 8$ unit cells along $[1000]$, $[2\bar{1}\bar{1}0]$ and $[0001]$, respectively, equivalent to 1920 atoms. Both carbon [(0001)-C]- and tungsten [(0001)-W]-terminated surfaces were considered.

The amorphous cells contained 1000 atoms and were created in a similar manner as the hydrogenated amorphous carbon samples used in Refs. 7, 16, and 17. Initially, W_xC_{1-x} samples with a tungsten content varying between $x=0.5$ and $x=0.9$ were created with a random distribution of carbon and tungsten atoms. Subsequently, the simulation cells were subjected to repeated cycles of temperature and pressure treatments until a configuration was obtained which was stable on the time scale of the simulations ($\sim$1 ns). The variation of the density with carbon content after the final equilibration at 300 K and 0 kbar is shown in Fig. 1. The densities for crystalline C, WC, and W as well as molten WC are included for comparison. The density of the stoichiometric amorphous structure lies below both the molten and crystalline phases, and as expected, the density increases with increasing tungsten content. Figure 2 shows the partial pair distribution functions for the as-created amorphous cells in comparison with the crystalline sample. In all cases, the first-neighbor peak is due to W-C or C-W pairs indicating that the components are well mixed. The position of the first-neighbor peak in the amorphous samples correlates approximately with the first-neighbor peak in the crystalline WC cell. The second-neighbor peak gradually shifts and splits with rising W content increasingly resembling the first- and second-neighbor peaks in bcc tungsten. Simultaneously, the relative weights

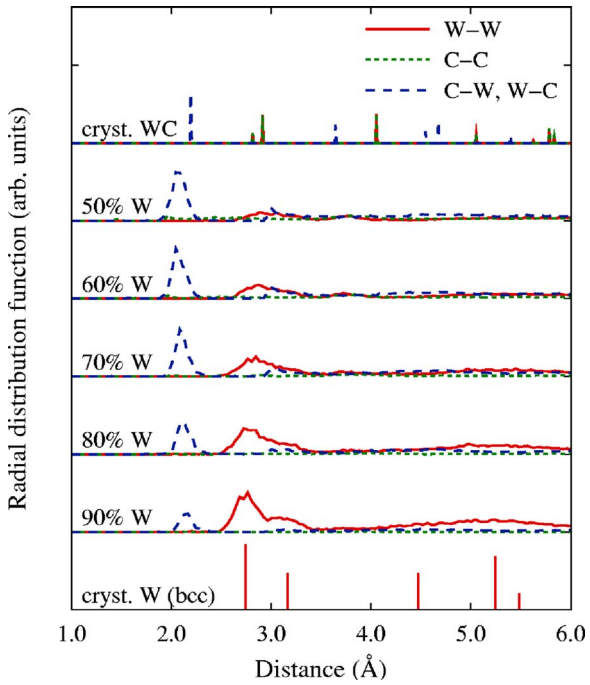

FIG. 2. (Color online) Total and partial pair distribution functions for the as-created amorphous cells as well as the crystalline sample. For comparison, the pair distribution function for bcc tungsten is shown as well.

of the first- and second-neighbor peaks decrease and increase, respectively. In general, pair correlations up to roughly the third-neighbor shell are observed. From the plots in Fig. 2, the range of the first-nearest-neighbor shells was deduced, which were used for calculating the coordination numbers shown in Fig. 7.

Initially, both crystalline and amorphous cells were equilibrated at 300 K and 0 kbar with periodic boundary conditions in all directions using the Berendsen temperature and pressure control.[18] Subsequently, free surfaces were created along the z direction (equivalent to the $[0001]$ direction for the crystalline cells), the pressure control was switched off, and the samples were once again thermalized at 300 K.

Before each individual bombardment simulation, a deuterium ion was placed above the surface at a distance larger than the maximum interaction range of the potential. The ion was assigned a certain speed and directed onto the surface at a randomly chosen angle of incidence between 0° and 20° from the surface normal, corresponding to the most common bombardment conditions in divertors. In order to achieve a uniform sampling of the surface, the cell was randomly shifted along the x and y directions before the bombardment was initiated. During bombardment, the atoms within 3 Å of the bottom of the cell were fixed and the atoms within a range of 5 Å were coupled to a Berendsen heat bath at 300 K in order to mimic the effect of an underlying bulk.

Both *noncumulative* and *cumulative* bombardment simulations were carried out. In the former case, the evolution of the system was followed for 5 ps and after each bombardment, the initial sample was restored. The cumulative simulations were performed in order to study the continuous damage buildup in the sample. Each bombardment simulation

was run for 5 ps followed by a 5 ps annealing run at 300 K. One series of simulation runs comprised 2000 ion impacts.

For the crystalline cells, the deuterium ion was assigned a speed equivalent to 10, 20, 50, 100, 200, 300, 1000, or 2000 eV in the cumulative bombardment simulations, and a speed equivalent to 50, 100, 600, or 2000 eV in the noncumulative simulations. For the amorphous samples, energies of 66 and 300 eV were used both in the cumulative and noncumulative simulations. The cells used in our simulations are too small to study the development of the full collision cascade for H ions with energy higher than 200 eV. Since the ions are light, dense collision cascades with ensuing strong pressure waves do not occur. Hence, the thermostating at the borders employed in our simulations is sufficient for the present purpose.

An atom was considered to be eroded if it was no longer bonded to the surface neither directly nor via its neighbor. Two atoms are bonded in the present model if their separation is smaller than the interaction range of the interatomic potential model used. For the noncumulative simulations, the sputtering yield is obtained as the average number of eroded C (W) atoms per incoming D ion and the standard deviation is calculated accordingly. For the cumulative simulations, the yield is determined by dividing the total number of eroded C (W) atoms in a simulation series by the total number of incoming D ions. The error bars in Fig. 3 are obtained by calculating the standard deviation over *all* individual bombardment events of a cumulative simulation series.

III. CRYSTALLINE TUNGSTEN CARBIDE

The carbon sputtering yields obtained from the cumulative simulations of (0001)-W and (0001)-C surfaces are shown in Fig. 3. Both surfaces display the same trend: The yield rises from close to zero at low bombardment energies, peaks for 100 eV, and thereafter decreases with increasing ion energy. For all energies, the erosion of tungsten is negligible which is equivalent to preferential sputtering of carbon, in agreement with experiment (see discussion below). While the sputtering yields for (0001)-C and (0001)-W are of the same order of magnitude, the former can be larger by as much as a factor of 4, since the carbon atoms in the first surface layer can react more easily with the incoming deuterium ions.

It is noteworthy that some erosion occurs for all energies, even for an energy as low as 10 eV for which the maximum possible energy transfer from a 10 eV D to a surface carbon atom is only 4.9 eV. Since this value is much smaller than the cohesive energy of bulk WC (−16.8 eV/f.u.), ordinary physical sputtering, which for the present case requires an energy of at least ~50 eV, cannot account for the observed erosion. On the other hand, visual inspection of the evolution of the simulation cells during bombardment shows that the erosion of carbon and carbon-containing molecules is enhanced because of swift chemical sputtering, which is known to govern erosion at energies much below the threshold for physical sputtering.[7,19,20] This mechanism requires a sufficiently energetic hydrogenic ion to attack the region between two carbon atoms. The repulsive interaction between the incoming ion and the carbon atoms can push the latter apart which causes breaking of the covalent bond and potentially sputtering of the carbon atoms. This effect is further amplified at the (0001)-C surface, where the C atoms have only three bonds to the underlying W layer (the C atoms within the layer are too far apart to form covalent bonds with each other). These atoms can, therefore, be eroded at relative ease by swift chemical sputtering.

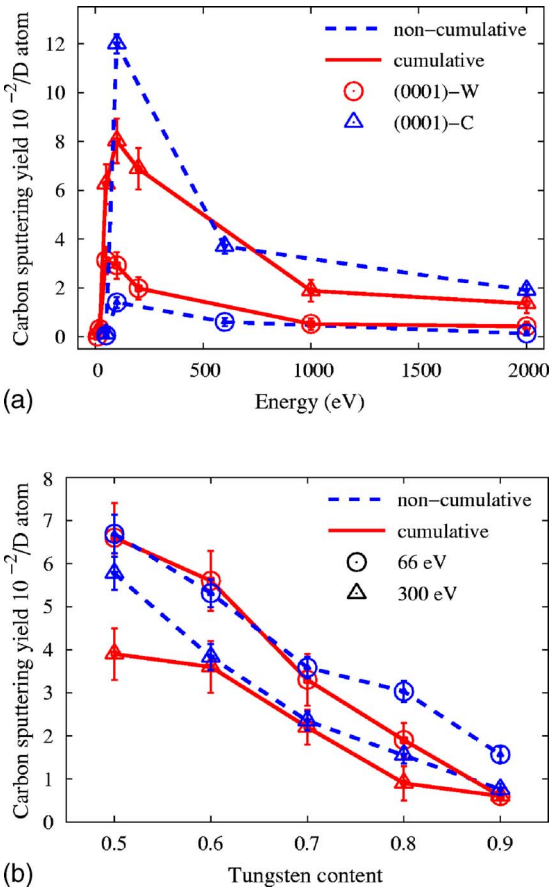

FIG. 3. (Color online) Carbon sputtering yields calculated obtained from cumulative and noncumulative bombardment simulations of deuterium impinging onto (a) crystalline and (b) amorphous sample cells of tungsten carbide. The sputtering of tungsten is practically negligible. The error bars show the standard deviation calculated over all individual bombardment events.

The snapshots of the cells at the end of the cumulative simulations (Fig. 4) show amorphization of the surface for energies between ~50 and 200 eV. The amorphization is the most pronounced at an energy of 100 eV corresponding to the maximum in the yield. During the course of the simulation, carbon molecules formed due to amorphization of the surface are subject to erosion by swift chemical sputtering.[7,19] For energies below ~50 eV and above 200 eV, the crystalline structure remains largely intact. Energies below 50 eV are obviously too small to cause (nonrecoverable) bulk damage. On the other hand, for energies above ~200 eV, the maximum of the depth distributions of the energy and the deposited ions exceeds the vertical size of the simulation cells used in the current simulations.

We have further analyzed the distribution of deuterium within the cells after cumulative bombardment, as shown in

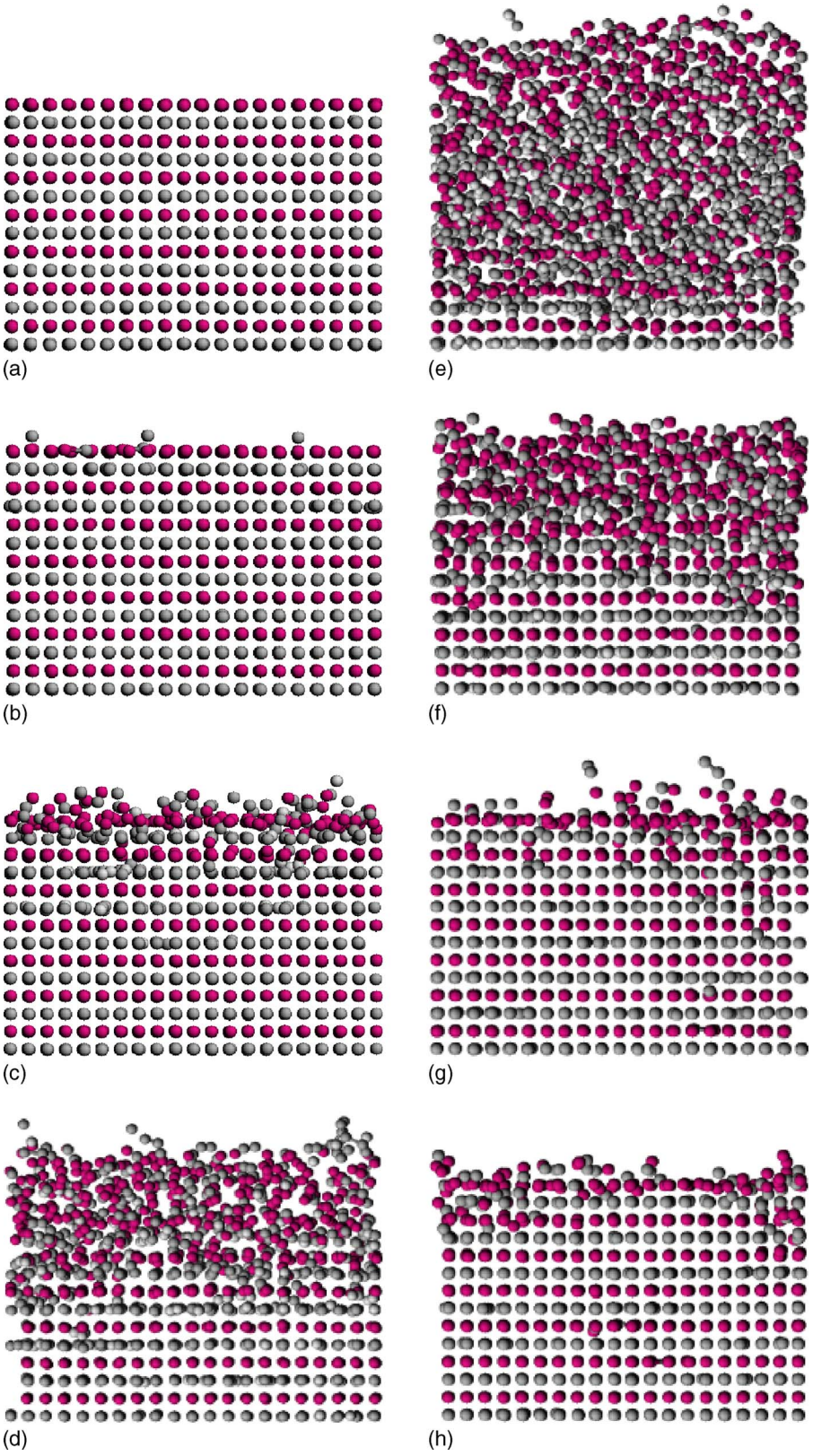

FIG. 4. (Color online) Snapshots of the (a) first and [(b)–(h)] last frames of the WC lattice after cumulative deuterium bombardment with 2000 ions at (b) 10 eV, (c) 20 eV, (d) 50 eV, (e) 100 eV, (f) 200 eV, (g) 1 keV, and (h) 2 keV. The lighter spheres represent C atoms and the darker ones W atoms.

Fig. 5. The tungsten-terminated surface displays an almost twice as large retention of deuterium as the carbon-terminated surface which is related to the larger sputtering yield of the latter (note that in the chemical sputtering mechanism, most sputtered species are hydrocarbon molecules). The more deuterium is consumed in surface reactions, the less reaches the bulk of the sample where it can be retained. The deuterium profiles are rather broad and the depth at which most of the deuterium is deposited scales roughly with the energy of the incoming particle. (Note that

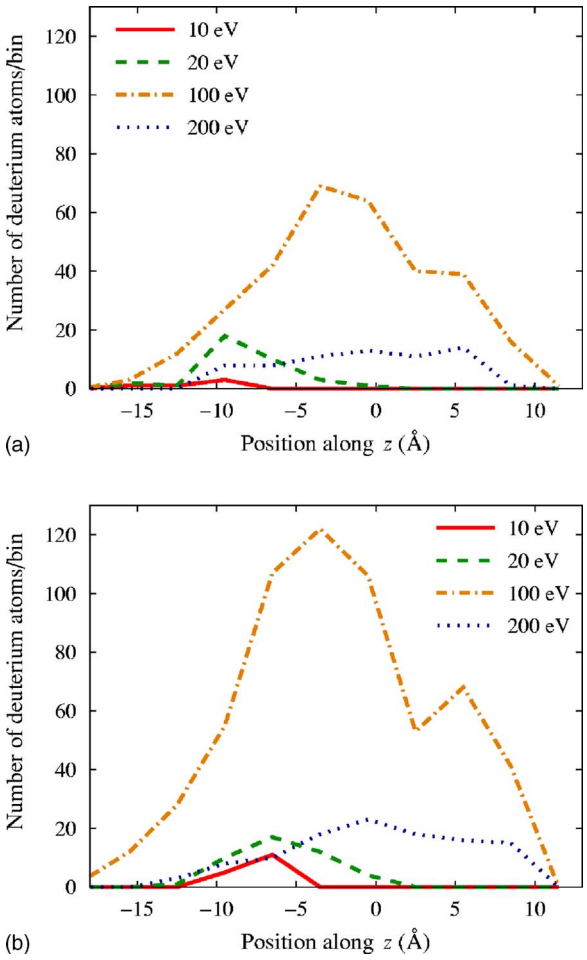

FIG. 5. (Color online) Depth distribution of deuterium after bombardment with 2000 ions for (a) the (0001)-C and (b) the (0001)-W surface. Note that for the 1 and 2 keV cases, the maximum in the deuterium profile would not be visible in the plot, and hence, the curves for these energies are not shown. The bin size was 3 Å. The areas below the curves are not the same because at low energies, many D atoms are reflected off the surface or chemically eroded, and at high energies, they start to be transmitted through the cell.

for the 1 and 2 keV cases, the maximum in the deuterium profile is not visible in the plot.) Compared with results obtained from SRIM calculations (where only physical sputtering is described), we note similar sputtering yields as the molecular dynamics (MD) simulations at higher energies, where chemical sputtering plays a minor role. In Fig. 6, the energy distribution and the range distribution of bombarding deuterium ions using SRIM are compared. As can be seen from the plot, more energetic D atoms transfer more energy to the atoms in the sample, but the maximum in the range distribution is also located deeper in the box. Compared with the degree of amorphization and the damage production shown in Fig. 4, we note that the recoil energy transfer from the deuterium ions is not enough to describe the amorphization of the sample, but that the retained deuterium causes the sample to amorphize more easily at 100 eV than at 200 eV. Further analysis shows that for the 100 eV bombardment case, for which the deuterium retention assumes a maximum,

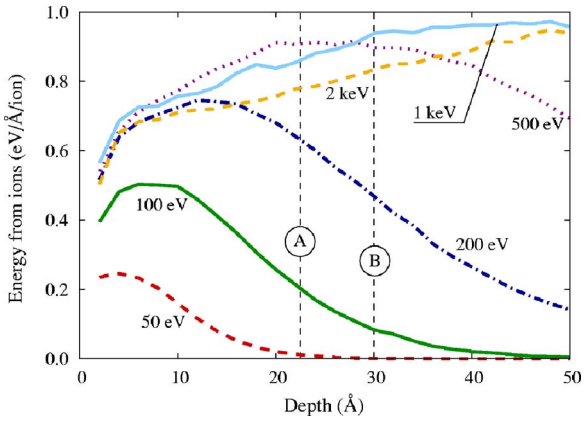

FIG. 6. (Color online) Energy vs depth distribution as obtained from SRIM calculations. The simulation cell sizes are marked with dashed lines: (A) crystalline and (B) amorphous samples.

a particular large fraction (33%–48%) of the deuterium is bound as D_2 "molecules" inside the solid. These atoms were filtered according to a distance criterion ($r_{D\text{-}D} \leqslant 1.7$ Å, maximum cutoff distance of the potential) in combination with an energy criterion (sum of atomic energies within 0.3 eV of the dimer energy of 4.75 eV). On the other hand, in the 50 and 200 eV cases, the fraction of deuterium atoms in D_2 molecules is only about 13% and 7%, respectively.

Figure 7 shows the distribution of coordination numbers for tungsten, carbon, and hydrogen after bombardment of the (0001)-C surface with deuterium ions at an energy of 100 eV. The average coordination numbers for both tungsten and carbon are smaller than in the perfect crystal which correlates with a lowering of the density. Most of the carbon is still sixfold coordinated as in crystalline WC but a considerable amount of three and fourfold-coordinated C atoms points to the formation of sp^2 and sp^3 hybrids. The tungsten atoms are predominantly 13- to 14-fold coordinated compared to a coordination number of 14 in both tungsten carbide and metallic tungsten.

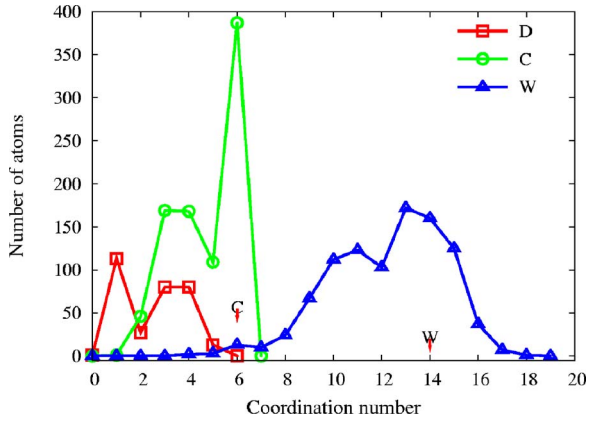

FIG. 7. (Color online) Distribution of coordination numbers for carbon, tungsten, and deuterium after bombardment of the (0001)-C surface with 2000 deuterium ions at an energy of 100 eV. The arrows mark the coordination numbers of W and C in crystalline tungsten carbide.

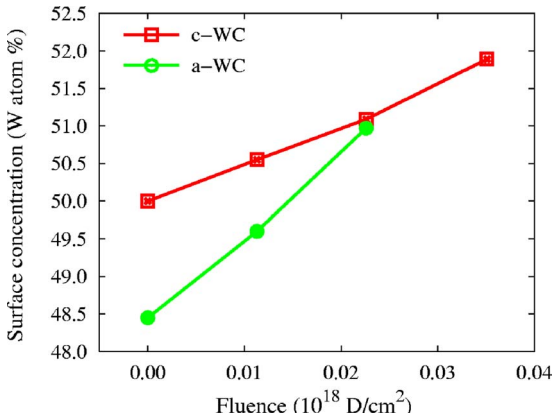

FIG. 8. (Color online) Illustration of the buildup of the W concentration in both the crystalline (*c*-WC) and the stoichiometric amorphous (*a*-WC) cell.

IV. AMORPHOUS TUNGSTEN CARBIDE

The carbon sputtering yields obtained from our cumulative and noncumulative simulation runs with five different amorphous tungsten carbide cells are plotted in Fig. 3(b). The carbon sputtering yields are decreasing with increasing tungsten content of the cell. The tungsten sputtering yields are zero within the statistical uncertainties. Larger sputtering yields are obtained for 66 eV than for 300 eV. The amount of deuterium trapped in the sample cell varies with the carbon/tungsten concentration of the cell. For the lower investigated energy, 66 eV, we observe a saturation in the deuterium concentration after about 1500 incoming particles. It must be noted that the presence of an "infinite" bulk and a longer time between impacts could, at least at elevated temperatures, allow the deuterium to diffuse away such that saturation would not be reached. The simulations are, however, constrained due to the finite extent of the cells along z and the limited molecular dynamics time scale.

V. DISCUSSION

For the crystalline cells, we made the following observations: The surface damage increases with increasing energy up to a maximum value at about 100 eV after which it decays again. After 1500 cumulative simulation events, the cells bombarded at 10 and 2000 eV show a similar amount of damage; the carbon sputtering yields are similar as well. This is expected from basic nuclear stopping theory;[21] right at the surface, the nuclear energy deposition is low for high energies, resulting in little damage and sputtering. The MD results show large sputtering yields for C at low energies, while at higher energies, the C yields approach those predicted by SRIM,[22] a computer code which only describes physical sputtering.

In both cumulative and noncumulative simulations, the W sputtering yield is very low ($\ll 0.01$). This implies that C is sputtered preferentially. The preferential sputtering of C naturally leads to a buildup of the W at the surface. This is illustrated in Fig. 8 which shows the W surface concentration $c(\phi)$ in the crystalline, W-terminated surface and the amorphous $W_{0.5}C_{0.5}$ surface as a function of ion fluency ϕ for 300 eV D ions. The surface concentration was evaluated by averaging all atoms in the simulation cell.

We now try to relate the data in Fig. 8 with the W surface concentration during 300 eV D bombardment measured by Plank and Eckstein using Auger electron spectroscopy.[10] Since the electron penetration curve is not a smooth function of depth, and not all experimental details are reported, it is not possible to compare our data directly with the experiment. Moreover, the highest doses we can achieve ($\sim 0.03 \times 10^{18}$ ions/cm^2) are below the experimental ones. However, in the experiments, the $c(\phi)$ data are linear with dose ϕ at the smallest doses. Assuming that in our simulation samples (equivalent to a 20 Å thick surface layer) the derivative $dc/d\phi$ is independent of depth, we can compare simulation and experiment.

In order to facilitate this comparison, we scanned in the experimental data from Fig. 5 in Ref. 10 and fitted a linear curve to the lowest-dose data. Thereby, we obtained an experimental value for $dc/d\phi = 63 \pm 10$ at. %/(10^{18} ions/cm^2). Equivalently, from the simulated data shown in Fig. 6, we derived a value of $d\phi/dc = 57 \pm 7$ at. %/(10^{18} ions/cm^2) for the crystalline and a value of $d\phi/dc = 110 \pm 10$ at. %/(10^{18} ions/cm^2) for the amorphous cells. The good agreement between experiment and simulation demonstrates the suitability of our model and provides a strong support for the validity of our results.

Note that the C sputtering yields obtained in our simulations cannot be compared directly with those reported in other experiments.[2–14] The doses employed in other experiments have been so high that even if the experiments started with stoichiometric WC, most of the sputtering occurred after the preferential sputtering had removed most of the C from the surface layers.

Physical (ballistic) sputtering can only occur above a certain threshold energy which in the present case is ~ 50 eV. We do, however, observe significant carbon sputtering well below this energy which can be explained by swift chemical sputtering.[20] On the other hand, the W yields remain low since W is a metal which prefers high coordination numbers and hence does not easily sputter by the swift chemical sputtering mechanism. The physical sputtering yields for W by D are experimentally known to be very low ($\ll 0.01$) in pure tungsten.[23] Since W and WC have comparable cohesive energies, the physical sputtering yield of W from WC can be expected to be comparably small, in agreement with our simulation results.

VI. CONCLUSIONS

We have studied the behavior of WC under low-energy deuterium bombardment for crystalline as well as amorphous surfaces by means of molecular dynamics simulations. Both cumulative and noncumulative simulation runs were performed. Prolonged bombardment leads to the formation of an amorphous WC surface layer, regardless of the initial structure of the WC sample. Hydrocarbons formed at the surface of these amorphous layers can erode by swift chemical sputtering. Larger sputtering yields are obtained from carbon-

terminated surfaces than from tungsten-terminated surfaces. In both cumulative and noncumulative simulations, C is observed to sputter preferentially.

The results obtained in this paper have important implications for mixed material erosion in fusion reactors. Just like C-based materials, WC-like materials can be expected to be subject to chemical erosion down to very low energies of impinging deuterium or tritium particles. This is in contrast to pure W, which does not erode due to chemical sputtering.

In agreement with experiment, we observe preferential sputtering of carbon. This suggests that WC layers formed by C redeposition will be reduced in C content if subjected to hydrogen/deuterium bombardment. Hence, if a section of the reactor first wall is subject to both redeposition of hydrocarbons and hydrogen bombardment, a dynamic balance in the C content could be reached under prolonged operation.

ACKNOWLEDGMENTS

This work was supported by Association Euroatom-TEKES under the FUSION program, and the Magnus Ehrnrooth Foundation. Grants of computer time from the Center for Scientific Computing in Espoo, Finland are gratefully acknowledged. We also acknowledge financial support through a bilateral travel program funded by the German foreign exchange server (DAAD) and the Academy of Finland (Project No. 204461).

[1] K. Do-Heyoung, Y. J. Kim, Y. S. Song, B.-T. Lee, J. H. Kim, S. Suh, and R. Gordonc, J. Electrochem. Soc. **150**, C740 (2003).
[2] G. Montay, A. Cherouat, A. Nussair, and J. Lu, J. Mater. Sci. Technol. **20**, 81 (2004).
[3] K. Kurihara, K. Sasaki, M. Kawarada, and Y. Goto, Thin Solid Films **212**, 164 (1992).
[4] R. Tivey, T. Ando, A. Antipenkov, V. Barabash, S. Chiocchio, G. Federici, C. Ibbott, R. Jakeman, G. Janeschitz, R. Raffray, M. Akiba, I. Mazul, H. Pacher, M. Ulrickson, and G. Vieider, Fusion Eng. Des. **46**, 207 (1999).
[5] H. Maier and ASDEX Upgrade Team, J. Nucl. Mater. **335**, 515 (2004).
[6] J. Kuppers, Surf. Sci. Rep. **22**, 249 (1995).
[7] E. Salonen, K. Nordlund, J. Keinonen, and C. H. Wu, Phys. Rev. B **63**, 195415 (2001).
[8] W. Wang, J. Roth, S. Lindig, and C. H. Wu, J. Nucl. Mater. **299**, 124 (2001).
[9] D. P. Coster, X. Bonnin, B. Braams, D. Reiter, R. Schneider, and the ASDEX Upgrade Team, Phys. Scr., T **T108**, 7 (2004).
[10] H. Plank and W. Eckstein, Nucl. Instrum. Methods Phys. Res. B **124**, 23 (1997).
[11] W. Wang, V. K. Alimov, B. M. U. Scherzer, and J. Roth, J. Nucl. Mater. **241-243**, 1087 (1997).
[12] M. I. Guseva, A. L. Suvorov, S. N. Korshunov, and N. E. Lazarev, J. Nucl. Mater. **266-269**, 222 (1999).
[13] M. I. Guseva, S. N. Korshunov, A. L. Suvorov, and N. E. Lazarev, Tech. Phys. **44**, 1123 (1999).
[14] M. Tanihuchi, K. Sato, K. Ezato, K. Yokoyama, M. Dairaku, and M. Akiba, J. Nucl. Mater. **313-316**, 360 (2003).
[15] N. Juslin, P. Erhart, P. Träskelin, J. Nord, K. Henriksson, E. Salonen, K. Nordlund, and K. Albe, J. Appl. Phys. **98**, 123520 (2005).
[16] E. Salonen, K. Nordlund, J. Tarus, T. Ahlgren, J. Keinonen, and C. H. Wu, Phys. Rev. B **60**, R14005 (1999).
[17] P. Träskelin, K. Nordlund, and J. Keinonen, Nucl. Instrum. Methods Phys. Res. B **228**, 319 (2005).
[18] H. J. C. Berendsen, J. P. M. Postma, W. F. van Gunsteren, A. DiNola, and J. R. Haak, J. Chem. Phys. **81**, 3684 (1984).
[19] E. Salonen, K. Nordlund, J. Keinonen, and C. H. Wu, Europhys. Lett. **52**, 504 (2000).
[20] A. V. Krasheninnikov, E. Salonen, K. Nordlund, J. Keinonen, and C. H. Wu, Contrib. Plasma Phys. **42**, 451 (2002).
[21] J. F. Ziegler, J. P. Biersack, and U. Littmark, *The Stopping and Range of Ions in Matter* (Pergamon, New York, 1985).
[22] J. F. Ziegler, SRIM 2003 software package, available online at http://www.srim.org
[23] *Sputtering by Particle Bombardment I*, edited by R. Behrisch (Springer, Berlin, 1981).